Fluid Mechanics of Laminated Sheet Manufacture

I. Eames and N. Wright
Dept. of Mechanical Engineering, University College London, Torrington Place, London WC1E 7JE, U.K.

M. A. Gilbertson
Dept. of Mechanical Engineering, University of Bristol, University Walk, Bristol BS8 1TR, U.K.

The fluid mechanics of laminated sheet manufacture was studied by pouring a liquid filler from a point source onto an inclined moving sheet and then passing it under a narrow gap below a pinch bar that spreads the liquid under the influence of gravity. The liquid filler must pass under the pinch bar before it starts to solidify. The spreading of a viscous liquid as it undergoes this process was studied theoretically and experimentally. Steady similarity solutions were obtained based on a vertically averaged formulation of the mass and momentum equations for viscous flows. Experimental measurements of the spread of the fluid and the time taken for fluid to travel from the source to the pinch bar agreed well with theoretical predictions. The new models are applied to the operation of the manufacturing process and the implications are discussed.

Introduction

Many laminated materials consist of a soft, expanded filler encased in two tough, thin, and flexible sheets. The filler is applied as a liquid and spread in a layer between the two sheets before it expands and solidifies. There are several methods of achieving this, but one is shown in Figure 1. Here, the liquid filler is pumped onto an inclined plane over which the sheeting material that will form the bottom skin of the composite passes. At the bottom of the slope the liquid passes under a narrow gap formed by a pinch bar. The upper sheet of material passes around and under the edge of the pinch bar. The pinch bar has two purposes: first, the narrow gap causes the liquid to collect and spread out sideways over the full width of the machine; secondly, the bar enables the liquid to be spread evenly. Immediately before being introduced onto the inclined slope the filler is activated (by adding a chemical agent) so that it starts to solidify and form a rigid board. This might typically take place after about 10 s.

The process just described for making a laminated board is poorly understood. Manufacturers often set their machine through trial and error; however, any change in operating conditions can result in an increase in the travel time or the liquid from its introduction until its passage under the pinch bar. This may cause subseqent problems associated with the premature solidification of the filler. The aim of the work described in this article was to understand the spreading of a viscous liquid under the influence of gravity and, in particular, the factors that influence the maximum travel time of the fluid from the source to when it has passed under the pinch bar. The process has been analyzed mathematically and experimentally. Rather than attempt to reproduce the complex, rapidly changing, and poorly understood rheology of the reacting fluids used in the actual process, the behavior of a generic liquid with a uniform but high viscosity was examined. The results will contribute to the provision of a rational means for assessing and optimizing the design of the manufacturing process.

A distinction can be made between the passage of the fluid down the slope over which a moving piece of material is passing and the lateral spreading of the liquid in front of the pinch bar under which it ultimately passes. The flow of a thin film of fluid can be described by the general lubrication equation, which balances viscous forces with gravity, surface tension, long-range molecular forces, and surface-tension gradients (Myers, 1998). The study of the coating of a moving sheet with a liquid where surface tension is dominant is well developed and described by the Landau–Levich equation, which balances the advection of a viscous liquid by the moving sheet with surface tension to give (Myers, 1998)

$$Ch^3\frac{\partial^3 h}{\partial x^3} - 3Uh = -3Uh_\infty \qquad (1)$$

Correspondence concerning this article should be addressed to I. Eames or M. A. Gilbertson.

where C is the ratio of surface tension to viscous forces, h_∞ is the equilibrium film thickness, and U is the speed of the surface. A number of researchers have examined the spreading of a viscous fluid on horizontal, rigid surfaces (Didden and Maxworthy, 1982; Huppert, 1982a) using a combination of scaling and similarity analysis, and experimental measurements. This analysis was developed further by Huppert (1982b) and, in a comprehensive study, by Lister (1992) for the spreading of viscous fluid down a fixed rigid surface. These considerations have been extended to consider the spread of fluids over rigid horizontal surfaces whose viscosity increases with time owing to cooling, such as lava (Bercovici, 1994). This article considers the spreading of viscous fluid from a point source located above a rigid moving surface and then the fluid flow parallel to the pinch bar. This treatment is supported by an experimental study using a full-scale model of the manufacturing plant (that is, with overall dimensions of the order of two meters), which was used to generate data for comparison with the theoretical predictions.

This article is structured as follows. In the subsection "The flow of a viscous liquid down an inclined surface," the analyses of Lister (1992) are discussed in relation to flow down a fixed inclined surface and new similarity solutions are derived to describe the spreading of a flow from a point source above a moving surface. The lateral flow of the viscous fluid near the pinch bar is analyzed in the next subsection. The experimental study is described in the third section, and the results correlated with theoretical predictions. The consequences of the results for the production of laminates are discussed in the fourth section. Conclusions are drawn in the final section.

Mathematical Description

The flow of a viscous liquid down an inclined surface

The flow of a viscous liquid down an inclined surface over which a continuous sheet of material is passing is shown in Figure 1. The z-axis is perpendicular to the moving surface and the x-axis is in its direction of travel. When inertial forces are negligible compared to viscous forces, the dynamic balance on the liquid is between viscous forces and the gradient of pressure, and this is described by

$$\mu\nabla^2\boldsymbol{u} = \nabla p - \rho g\hat{\boldsymbol{x}}\sin\theta \tag{2}$$

The layer of fluid is thin so that the thickness of the flow perpendicular to the direction of its propagation is negligible compared to its length; thus, the horizontal gradients of velocity are much smaller than its vertical gradient and

$$\mu\frac{\partial^2\boldsymbol{u}}{\partial z^2} = \nabla p - \rho g\hat{\boldsymbol{x}}\sin\theta \tag{3}$$

where the vector operations are now in two dimensions. The pressure in the fluid is hydrostatic and increases from the atmospheric pressure, p_0, at the top of the current ($z = h$) to a maximum at the bottom of the fluid ($z = 0$) so that when the density of the flow is much larger than that of the ambient fluid

$$p = p_0 + \rho(h - z)g\cos\theta \tag{4}$$

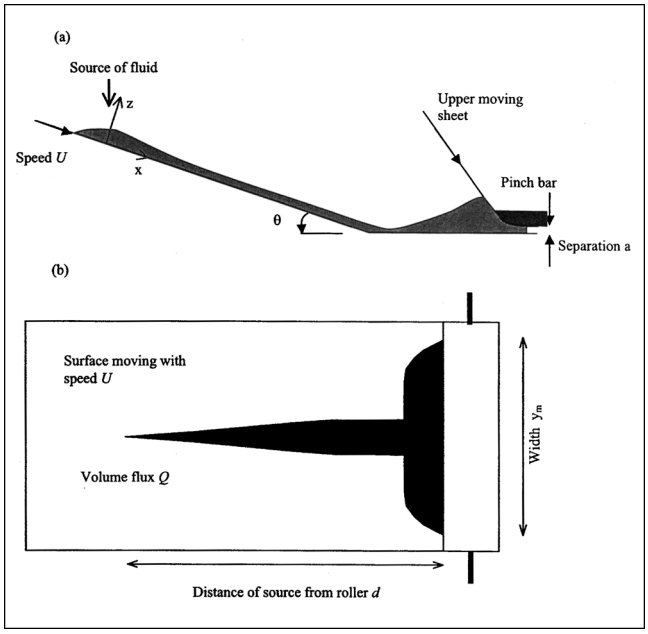

Figure 1. (a) Side view and (b) plan view of an industrial process where fluid is advected by a moving sheet of material toward a pinch bar where it forms a pool and spreads laterally.

where ρ is the density of the flowing fluid. Horizontal gradients of fluid pressure arise from variations of the fluid-layer thickness and when Eq. 4 is combined with Eq. 3

$$\mu\frac{\partial^2\boldsymbol{u}}{\partial z^2} = \rho g\cos\theta\nabla h - \rho g\hat{\boldsymbol{x}}\sin\theta \tag{5}$$

The flow is subject to two boundary conditions:

(1) A no-slip condition on the lower boundary: $\boldsymbol{u} = U\hat{\boldsymbol{x}}$, at $z = 0$.

(2) A zero-stress condition on the free-surface: $\partial\boldsymbol{u}/\partial z = \boldsymbol{0}$, at $z = h$.

Integration of Eq. 5 over the depth of the fluid and the application of boundary conditions yields

$$\bar{\boldsymbol{u}} = \left(\overline{u_x}, \overline{u_y}\right) = \frac{1}{h}\int_0^h \boldsymbol{u}\,dz = -\frac{h^2\rho}{3\mu}g[\cos\theta\nabla h - \sin\theta\hat{\boldsymbol{x}}] + U\hat{\boldsymbol{x}} \tag{6}$$

This may be coupled with the depth-averaged mass conservation equation

$$\frac{\partial h}{\partial t} + \nabla\cdot\left(h\bar{\boldsymbol{u}}\right) = 0 \tag{7}$$

to yield a nonlinear advection diffusion equation with a form similar to the general lubrication equation (Myers, 1998)

$$\frac{\partial h}{\partial t} = \frac{\rho g \cos\theta}{3\mu}\frac{\partial}{\partial y}\left(h^3\frac{\partial h}{\partial y}\right) + \frac{\rho g \cos\theta}{3\mu}\frac{\partial}{\partial x}\left(h^3\frac{\partial h}{\partial x}\right) - \frac{\rho g \sin\theta}{3\mu}\frac{\partial h^3}{\partial x} - U\frac{\partial h}{\partial x} \quad (8)$$

This formulation is similar to that, for example, of Lister (1992), except that an advection term is included on the righthand side of Eq. 8. From this equation it is possible to analyze a number of situations such as the spread of a liquid on a horizontal surface, the effect of inclining the surface, and the further changes induced by the movement of the surface. We shall concentrate on steady solutions.

Spread of Viscous Fluid from a Point Source on an Inclined Rigid Surface. The flow of a viscous liquid down a moving inclined surface is governed by Eq. 8. Two extremes can be considered: first, the liquid travels independently of the moving surface, so that it is effectively traveling as if the surface were stationary; second, the liquid is wholly advected by the belt.

In the first case, the flow down a fixed inclined surface ($U = 0$) from a steady source, the motion of the fluid is determined by a balance between cross- and down-slope transport, the first and third terms on the righthand side of Eq. 8. The second term on the righthand side of Eq. 8 can be neglected in relatively broad, shallow flows on inclined surfaces when $\partial h/\partial x \ll \tan\theta$. This yields for a steady flow (Lister, 1992)

$$\cot\theta\frac{\partial}{\partial y}\left(h^3\frac{\partial h}{\partial y}\right) = \frac{\partial h^3}{\partial x} \quad (9)$$

When the length-scale that characterizes the width of the wetted region is denoted by Y, and that which characterizes its height by H, the order of magnitude of the terms in Eq. 9 can be estimated to be (Lister, 1992)

$$\cot\theta\frac{H^4}{Y^2} \sim \frac{H^3}{x} \quad (10)$$

The conservation of mass requires the downslope flux of fluid to be $Q \sim u_x HY$, and by using this in conjunction with Eq. 10 Lister (1992) showed that the viscous fluid spreads according to

$$Y \sim \left(\frac{3\mu Q\cos^3\theta}{\rho g \sin^4\theta}\right)^{1/7} x^{3/7}, \quad H \sim \left(\frac{3\mu Q}{\rho g\cos\theta}\right)^{2/7} x^{-1/7} \quad (11)$$

When the liquid is released onto a moving surface, the speed of the fluid relative to the surface decreases rapidly as it moves from the source until it is advected at a constant speed by the moving surface. This corresponds to the second case described earlier, and when the flow is shallow the downslope gradients of hydrostatic pressure can be neglected so that far from the source the steady flow is determined by a balance between the first and last terms on the righhand side of Eq. 8 and

$$\frac{\rho g\cos\theta}{3\mu}\frac{\partial}{\partial y}\left(h^3\frac{\partial h}{\partial y}\right) = U\frac{\partial h}{\partial x} \quad (12)$$

Equation 12 is similar to that describing planar viscous flow on a horizontal fixed surface, where x/U is replaced by time (Huppert, 1982a). This balance applies if $UH/x \gg \rho g H^3 \sin\theta/x\mu$ so that $U \gg \rho g H^2 \sin\theta/\mu$. Clearly this inequality will apply if the effect of the belt movement is much greater than that of gravity, which will be true when the current is shallow, the angle of the slope is small, or the liquid is sufficiently viscous. Under these conditions it then can be shown as be-

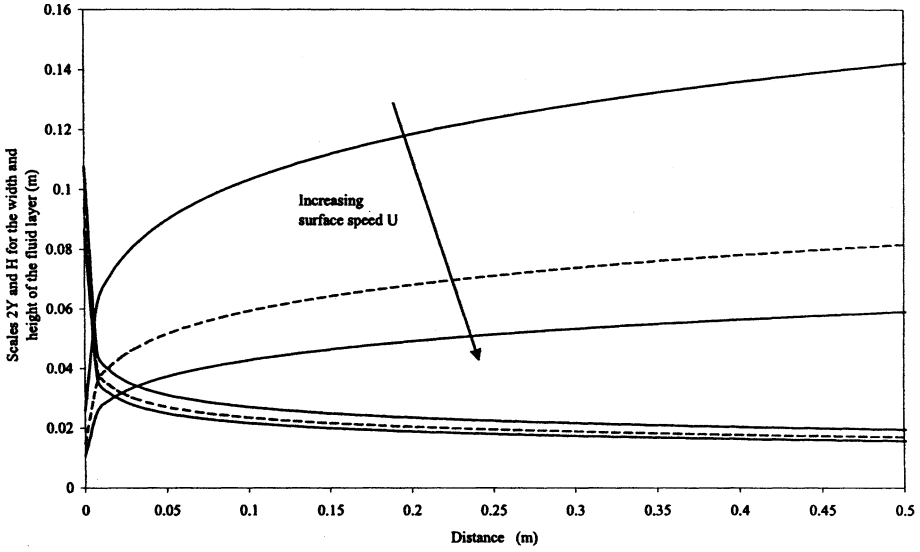

Figure 2. Spreading of a viscous fluid down a rigid surface moving with speed $U = 0.1$, 0.2, and 0.3 m/s.

The volume flux is $Q = 7.7\times10^{-5}$ m^3/s, viscosity $\mu = 1.9$ kg/ms, density $\rho = 1{,}200$ kg/m^3, and inclination $\theta = 15°$. The scales for the total width $2Y$ (top set of lines) and the center line height H (bottom set of lines) of the fluid layer are predicted by the similarity solution (Eq. 13).

fore from scaling analysis that liquid on the moving surface spreads as

$$Y = \left(\frac{5\rho g \cos\theta}{24\mu} \frac{Q^3}{U^4} \right)^{1/5} x^{1/5}, \quad H = \left(\frac{3\mu}{20\rho g \cos\theta} \frac{Q^2}{U} \right)^{1/5} x^{-1/5} \tag{13}$$

By expressing $\tilde{y} = y/Y(x)$ and $\tilde{h}(\tilde{y}) = h(x, y)/H(x)$, the nonlinear partial differential equation (Eq. 12) can be reduced to a nonlinear ordinary differential equation

$$\frac{d}{d\tilde{y}} \left(\tilde{h}^3 \frac{d\tilde{h}}{d\tilde{y}} \right) = - \left(\tilde{h} + \tilde{y} \frac{d\tilde{h}}{d\tilde{y}} \right) \tag{14}$$

with an integral constraint $\int_0^\lambda \tilde{h}\, d\tilde{y} = 1$. The width of the fluid layer is $\lambda Y(x)$, where λ is to be determined. Equation 14 can be integrated, and with the application of the boundary conditions $d\tilde{h}/d\tilde{y}\,|_{\tilde{y}=0} = 0$ and $\tilde{h}(\lambda) = 0$, gives

$$\tilde{h}(\tilde{y}) = \left(\frac{3}{2} \right)^{1/3} \left(\lambda^2 - \tilde{y}^2 \right)^{1/3} \tag{15}$$

where

$$\lambda = \left(\frac{2}{3} \right)^{1/5} \left[\int_0^{\pi/2} \cos^{5/3} d\theta \right]^{-3/5} \approx 1.035$$

A downslope distance from the source x_*, can be defined where there is a transition from the viscous fluid flowing relative to the moving surface (described by Eq. 9) to it being advected by the surface (described by Eq. 12). This takes place when the third term on the righthand side of Eq. 8 is comparable with the fourth term and the first term, so that

$$x_* \sim \left(\frac{\rho g}{3\mu} \right)^{3/2} \frac{Q^2}{U^{7/2}} \frac{\sin^{7/2}\theta}{\cos^2\theta} \tag{16}$$

For typical values of parameters in the experiments ($Q = 3 \times 10^{-5}$ m^3/s, $\theta = 15°$, $\rho = 1200$ kg/m^3, $\mu = 1.9$ kg/m s) x_* has a value between $O(2\times10^{-2})$ and $O(4\times10^{-4})$ m as the belt speed, U, increases from 0.1 to 0.3 m/s.

The development of the flow described by Eq. 13 is shown in Figure 2 where the half-width of the wetted region increases with downslope distance for three values of surface speed $U = 0.1$, 0.2, and 0.3 m/s. The calculations show that the rate of lateral spread of the fluid is large close to the source, but becomes very small as the fluid moves away from it.

Flow parallel to pinch bar

After passing down the inclined slope, the fluid collects in front of the pinch bar under which the belts and fluid pass. The geometry of the pinch bar can often be complex, but in order to gain insight into the physical processes operating, the pinch-bar geometry is simplified so that it presents a straight, uniform edge perpendicular to the flow of the liquid. In addition it is assumed that the area of contact between the liquid pool and the upper belt is not sufficiently large to affect the fluid flow, that is, $h_m/x_m \ll \tan\alpha$, where α is the angle between the two belts.

The Reynolds number characterizing the flow perpendicular to the pinch bar is

$$Re \sim \frac{\rho |\boldsymbol{u} \cdot \nabla \boldsymbol{u}|}{\mu \left| \frac{\partial^2 \boldsymbol{u}}{\partial z^2} \right|} \sim \frac{\rho U^2/x_m}{\mu U/h_m^2} = \frac{U h_m^2}{\nu x_m}$$

where x_m is the width of the pool and h_m is its thickness at $x = 0$. When $Re \ll 1$, viscous stresses or linear drag at the surface are important and inertial forces are weak; in the opposite limit, $Re \gg 1$, turbulent drag is applicable. In the experimental study, the Reynolds number is estimated to be $Re \sim 0.1$, and so the approximation $Re \ll 1$ can be strictly applied.

The width of the pool of liquid that forms before the pinch bar is much smaller than its lateral extent so that $y_m \gg x_m$. Under this condition the gradients of hydrostatic pressure parallel to the pinch bar are much smaller than gradients perpendicular to it. The separation of the advection of the fluid down the slope described earlier, and the flow parallel to the pinch bar, means that fluid is introduced to this pool at a rate of Q at the center line, and a flux of $Q/2$ moves in either direction parallel to the pinch bar driven by horizontal gradients of fluid pressure. A vertically averaged description of the steady flow along the pinch bar results in Eq. 8, but with $\partial h/\partial t = 0$. At the center line of the apparatus there will be a transitional region (shown in Figure 1b) where the flows cannot be separated and interact with one another; however, where this region is small compared with the overall fluid layer—as in this case—its influence on the overall dynamics will be small. A complex vortex structure can exist in the pool and this also cannot be accounted for in the description; however, this should not prevent a reasonable estimate to be made of the travel time of the fluid, as the vortices will not interfere with the static forces driving the fluid sideways.

As the fluid flows along the pinch bar, the flow rate gradually reduces because material is removed at a rate Ua under the pinch bar. The half-width of the pool of liquid can be obtained simply from the mass balance between the volumetric flow rate Q at which fluid is added to the pool and the volumetric flow rate $2y_mUa$ at which it is removed. This yields

$$y_m = \frac{Q}{2Ua} \tag{17}$$

Thus, provided the fluid is not very deep so that its passage under the pinch bar is through advection by the moving belts, the cross-slope width of the wetted region, $2y_m$, is independent of the governing fluid mechanics.

In the absence of a pool of liquid in front of the pinch bar, for instance, when the belt speed is large or the flow rate of liquid low, the liquid flow will become more like a lubrication layer between the two belts. In the industrial process and the

experimental study, a deep pool of liquid forms in front of the pinch bar so that $h \gg a$ and there exists a free-surface gravity flow. Moreover, when the length scales—the cross-belt width (x_m) and the depth of the fluid layer (h_m)—can be separated, the flow perpendicular to the pinch bar is described by a balance between the viscous stress exerted by the moving belt [$O(\mu U/h^2)$] and the gradient of hydrostatic pressure [$O(\rho g \partial h/\partial x)$]. In the absence of the pinch bar, the flow profile will be parabolic. The presence of the pinch bar introduces a no-slip condition at $x = 0$ (the flow is driven vertically to the origin by the moving belt), which modifies the flow in this region. However, since the layer is quite thin, the influence of the pinch bar on the overall dimensions of the pool is small, and over most of the flow the vertically averaged momentum equation reduces to

$$U = \frac{\rho g}{3\mu} h^2 \frac{\partial h}{\partial x} \tag{18}$$

In addition, the results of the following analysis show that the dimensions of the pool and travel time of the fluid from the source to when it passes under the pinch bar depends on the leading coefficient of the preceding expression (which changes near the pinch bar) raised to the power of 1/7, so its overall influence will be small. Equation 18 describes the balance between fluid advection by the moving belt and the viscous spreading perpendicular to the pinch bar. Integration of Eq. 18 establishes the relation between h_m and x_m at any y-position,

$$x_m(y) = \frac{\rho g h_m(y)^3}{9\mu U} \tag{19}$$

From the conservation of mass, the rate at which the volume flux of fluid parallel to the pinch bar is diminished is described by

$$\frac{\partial}{\partial y}\left(\int_{-x_m(y)}^{0} h\overline{u_y}\, dx\right) = -Ua \tag{20}$$

which when integrated gives

$$\int_{-x_m(y)}^{0} h\overline{u_y}\, dx = Ua(y_m - y) \tag{21}$$

Therefore

$$Ua(y_m - y) = -\int_{-x_m(y)}^{0} \frac{\rho g}{3\mu} h^3 \frac{\partial h}{\partial y}\, dx = -\frac{\rho g}{12\mu}\frac{d}{dy}\int_{-x_m(y)}^{0} h^4\, dx \tag{22}$$

where the partial differential could be taken outside the integral sign because the integrand is identically zero at $x = -x_m(y)$. When Eq. 22 is integrated and the boundary condition $h = 0$ at $y = y_m$ is applied, the maximum height of the fluid layer at a distance y from the center line is

$$h_m(y) = \left(\frac{63}{2}\right)^{1/7}\left(\frac{\mu}{\rho g}\right)^{2/7}\frac{Q^{2/7}}{a^{1/7}}\left(1 - \frac{y}{y_m}\right)^{2/7} \tag{23}$$

From Eq. 19, the width of the fluid layer is

$$x_m(y) = \frac{1}{9}\left(\frac{63}{2}\right)^{3/7}\left(\frac{\rho g}{\mu}\right)^{1/7}\frac{Q^{6/7}}{a^{3/7}U}\left(1 - \frac{y}{y_m}\right)^{6/7} \tag{24}$$

Both the width and lateral extent of the fluid layer decrease inversely with the surface speed, whereas the thickness of the fluid layer is independent of U. Figure 3 shows how the size and shape of the liquid pool adjacent to the pinch bar varies with belt speed.

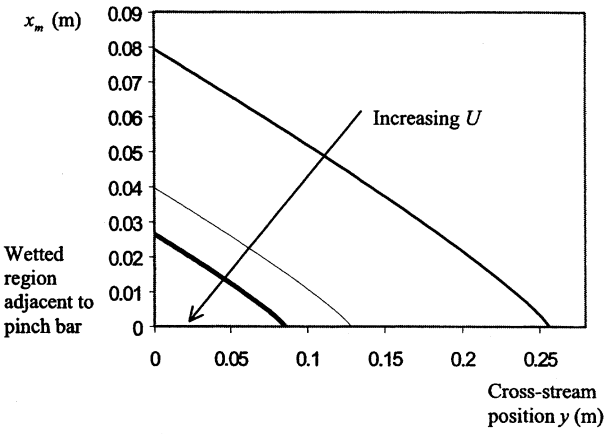

Figure 3. Shape of the liquid pool adjacent to the pinch bar according to the viscous flow theory (Eq. 24) for $U = 0.1$, 0.2, and 0.3 m/s.

The volume flux is $Q = 7.7 \times 10^{-5}$ m^3/s, viscosity $\mu = 1.9$ kg/ms, density $\rho = 1{,}200$ kg/m^3, and the pinch bar separation is a $a = 1.5 \times 10^{-3}$ m.

For Eq. 24 to be consistent with the initial assumption of the separation of scales ($x_m \ll y_m$), it is then required that

$$\frac{\mu Q}{\rho g a^4} \gg 1 \tag{25}$$

The smallest value of Q used in the experimental arrangement is $Q = 2 \times 10^{-5}$ m^3/s, with $a = 1.5 \times 10^{-3}$ m, so that the lefthand side of the preceding inequality is $O(10^3)$ and it is clearly satisfied. The variation with belt speed of the three dimensions of the fluid layer adjacent to the pinch bar—$h_m(0)$, $x_m(0)$, y_m—can be calculated as a function of belt speed and volume flux of liquid. It is also necessary for the width of the transitional region between flow perpendicular and flow parallel to the pinch bar to be small compared with the overall width of the flow, y_m. By comparison between Eqs. 13 and 17, this requirement is satisfied when the distance from the source to the pinch bar,

$$d \ll \frac{3}{20}\frac{\mu Q}{\rho U a^5 g \cos\theta}$$

a condition easily met for the parameters used in the experiments.

The speed of fluid parallel to the pinch bar is

$$\bar{u}_y = \frac{4}{21}\frac{U}{Q^{1/7}a^{4/7}}\left(\frac{\rho g}{\mu}\right)^{1/7}\left(\frac{63}{2}\right)^{3/7}\left(1-\frac{y}{y_m}\right)^{-1/7} \quad (26)$$

The speed increases rapidly with y and becomes unbounded at $y = y_m$. The thickness of the fluid layer decreases rapidly toward the outer edge of the fluid layer so that the Reynolds number associated with the flow $[O(\bar{u}_y h_m/\nu)]$ is still small.

Travel times

The maximum travel time for the liquid to pass from the source to under the pinch bar includes the time it takes the liquid to travel from the source to the pinch bar and then from the center line parallel to the pinch bar to the edge of the pool. When the fluid is rapidly accelerated to the speed of the moving belt after it is introduced (so that x_*, determined from Eq. 16, is small), the time, T_1, taken for material to be transported from the source to the pinch bar is advective time

$$T_1 = \int_0^d \frac{dx}{\bar{u}_x} = \frac{d}{U} \quad (27)$$

where d is the distance between the source of the liquid and the pinch bar; 0.65 m in the experimental apparatus. Once at the pinch bar, the maximum time taken for fluid to travel to a distance y from the center line of the flow is

$$T_2 = \int_0^y \frac{dy}{\bar{u}_y} = \frac{147}{32}\left(\frac{2}{63}\right)^{3/7}\frac{Q^{8/7}}{U^2 a^{11/7}} \times \left(\frac{\mu}{\rho g}\right)^{1/7}\left[1-\left(1-\frac{y}{y_m}\right)^{8/7}\right] \quad (28)$$

An estimate for the upper bound of the total time taken for fluid to pass beneath the pinch bar, T, is the addition of T_1 to T_2 for when the fluid has to travel to the extreme edge of the pool ($y = y_m$)

$$T = T_1 + T_2 = \frac{d}{U} + \frac{147}{32}\left(\frac{2}{63}\right)^{3/7}\frac{Q^{8/7}}{U^2 a^{11/7}}\left(\frac{\mu}{\rho g}\right)^{1/7} \quad (29)$$

Figure 4a shows the variation of T_2 with distance from the center line for $U = 0.1$, 0.2, and 0.3 m/s. Figure 4b shows the total travel time, T, and the contributions of T_1 and T_2.

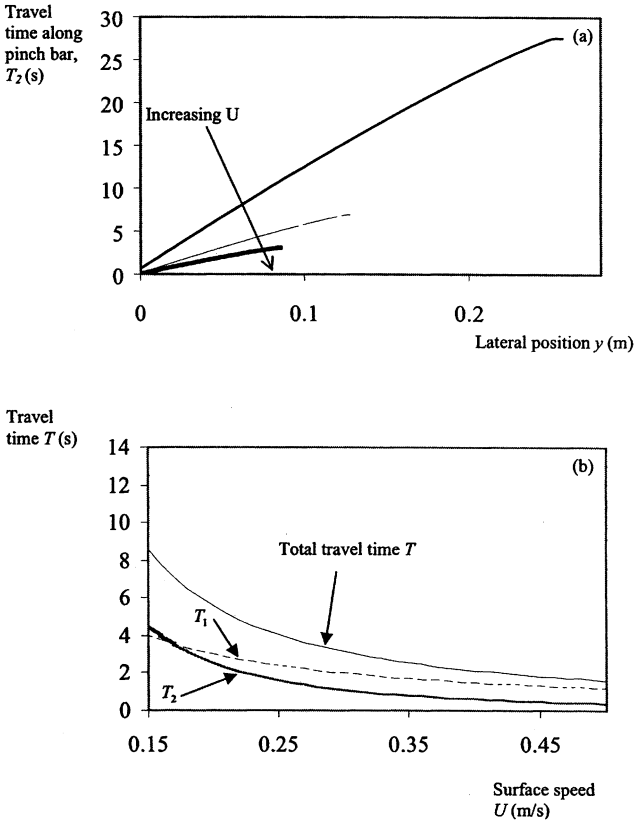

Figure 4. (a) Variation of the travel time T_2 along the pinch bar when $U = 0.1$, 0.2 and 0.3 m/s and the volume flux $Q = 7.7\times10^{-5}$ m^3/s.

The contributions to the total travel time T for $Q = 5.0\times10^{-5}$m^3/s as a function of surface speed are shown in (b) where the advection component is T_1.

Experimental Study

Experimental apparatus and procedure

Working Fluid. The fluid used in the experiments was a dilute sugar solution that was cheap, safe, easy to produce and use, and transparent. The fluid is essentially Newtonian, and it was possible to achieve large viscosities. The fluid used in the experiments had a viscosity of 1.97 ± 0.003 kg/ms. This fluid cannot simulate the unsteady, structured nature of the fluids used in the industrial process, but it does allow the effects of viscous flow on the evolution of the liquid pool to be clearly observed.

Release of Fluid onto a Moving Surface. A full-scale model of a machine for making laminates was constructed and is shown in Figure 5. It consisted of an adjustable steel frame with a number of rollers over which 1.30-m-wide polyurethane-coated belts passed. The belts and rollers were driven by an electric motor. The bed of the machine onto which the fluid was released was made from medium-density fiberboard. The upstream part of the bed could be inclined over a range of angles. The belt was held down in the inflection by a vacuum system. The belts ran below an aluminum pinch bar that fixed the gap through which liquid passed. The pinch bar could be raised or lowered by adjustment of its support, although accurate adjustment was difficult. The pinch-bar separation when the belts were stationary, measured with feeler gauges, was $a = 1.2\times10^{-3}$ m. When the apparatus was operated, the working fluid caused the pinch bar to flex slightly and the belt separation at the pinch bar then was estimated to be $a = 1.5\times10^{-3}$ m. The working fluid was contained in a header tank and delivered under gravity through a 0.032-m-diam hose. After passing under the pinch

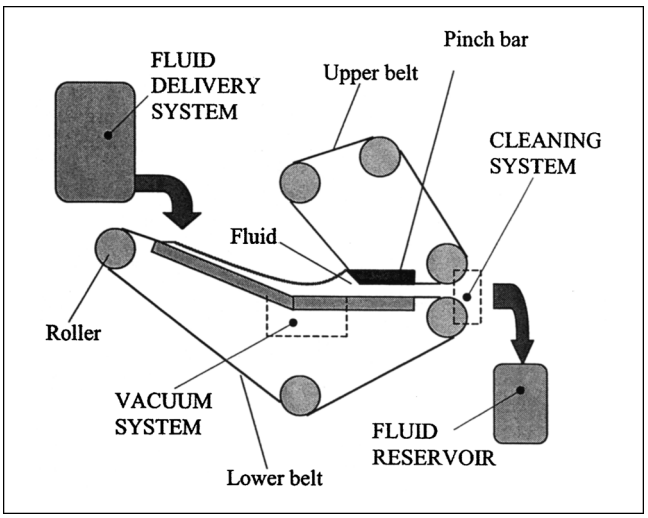

Figure 5. The experimental apparatus.

bar, the fluid was scraped off the belt by rubber blades and deposited in a reservoir.

The flow was made visible by the injection of dye into the fluid as it was released onto the moving belt. The capillary tube used to introduce the dye was regularly perforated along its length so that the fluid would be marked with a number of streams of dye across the whole flow. The experiments were videotaped for later analysis. Travel times were measured by the introduction of intermittent bursts of dye into the flow and the length of time during which they were visible through a frame-by-frame analysis of the video.

The parameter range of the experimental study is summarized in Table 1.

Experimental observations

Release of Liquid onto a Moving, Inclined Belt. The effect of a moving surface on the spreading of a viscous fluid is pronounced. This can be seen in Figure 6a where the spreading of liquid down a fixed surface is compared with that down a moving surface for the same volume flux of liquid. The scaling analysis just presented indicates that when the width of the fluid layer is denoted by $y_w(=\lambda Y)$, it varies according to $y_w \sim x^{3/7}$ for a fixed surface, Eq. 11, and $y_w \sim x^{1/5}$ for a moving surface, Eq. 13. Lines corresponding with the exponents in these expressions are included on the figure and show the significant effect of transport by the moving belts. In order that a detailed comparison can be made between the experimental measurements and theoretical predictions, the finite nature of the source of viscous fluid must be taken into account. (The theoretical calculations were based on the assumption of a point source.) When the width of the fluid

Table 1. Parameters of Experimental Study

Q (m^3/s)	U (m/s)	μ (kg/m·s)	ρ (kg/m^3)	a (m)
$0-1.05\times10^{-4}$	0.16–0.58	1.97	1,200	1.5×10^{-3}

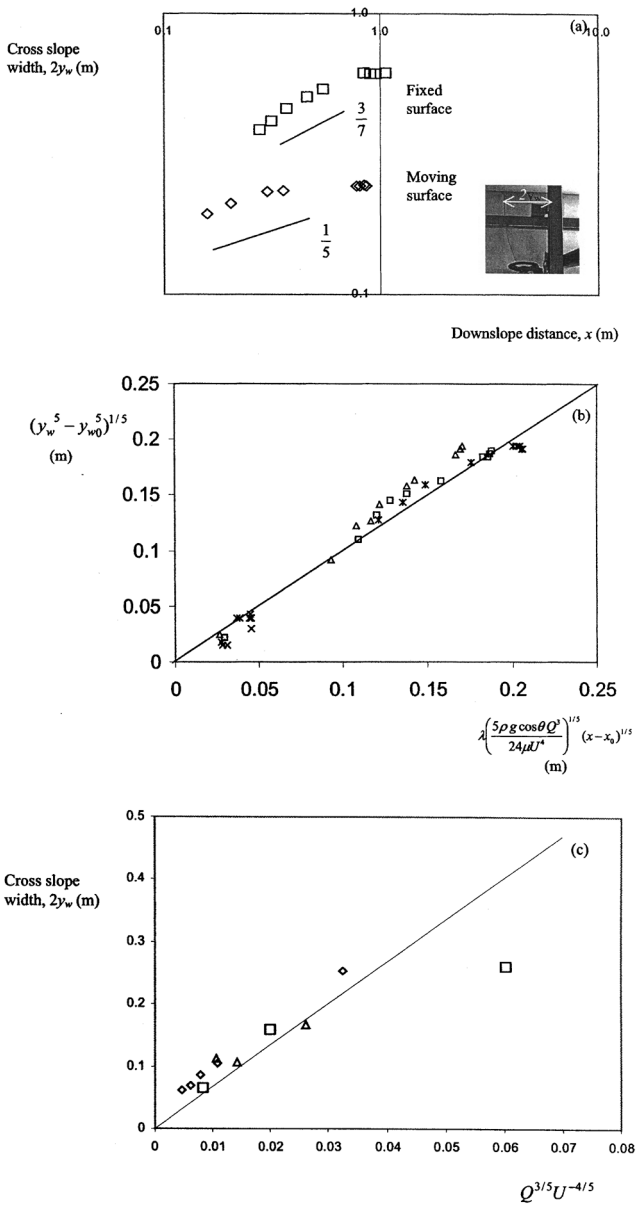

Figure 6. Comparison of the measured width of the fluid flow and model results (Eqs. 11 and 13).

(a) The contrast between the effect of moving and fixed surfaces on developing the fluid layer width with downslope position is shown. (b) Variation of width of the fluid layer with distance down the slope. The initial width of the fluid layer at a distance x_o from the source is $2y_{wo}$. The measurements were taken when $U = 0.1$ m/s. Volume flow rates Q, (×) 7.8×10^{-6}m^3/s; (△) 7.0×10^{-5} m^3/s; (□) 8.5×10^{-5} m^3/s; (∗) 9.95×10^{-5}m^3/s. The angle of the moving surface inclination to the horizontal is $\theta = 30°$. (c) The width of the fluid layer at a fixed position downslope ($x = 0.42$ m) as a function of volume flow rate Q and surface speed U for three values of volume flow rate: (□) 1.81×10^{-5} m^3/s, (◇) 3.63×10^{-5} m^3/s, and (△) 6.53×10^{-5} m^3/s.

layer is $y_w = y_{w0}$ at a distance $x = x_0$ from the finite area source, the spread of fluid is then described by

$$\left[y_w^5(x) - y_{w0}^5\right]^{1/5} = \lambda\left(\frac{5\rho g\,\cos\,\theta}{24\mu}\frac{Q^3}{U^4}\right)^{1/5}(x - x_0)^{1/5}, \quad (30)$$

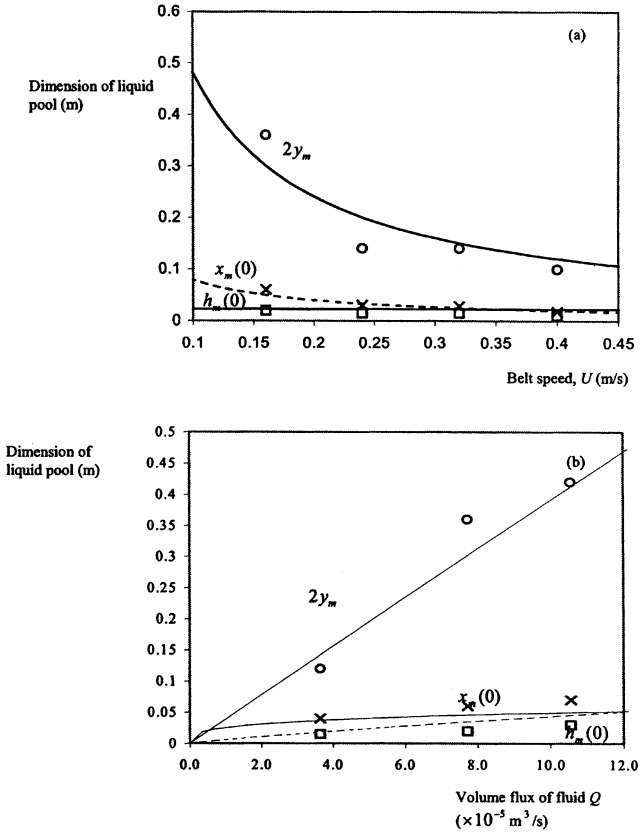

Figure 7. Measurements of the fluid pool dimensions in front of the pinch bar vs. model results (Eqs. 17, 23, 24) as a function of (a) surface speed with $Q = 7.7 \times 10^{-5}$ m^3/s and (b) volume flux with the belt speed fixed at $U = 0.16$ m/s.

which reduces to Eq. 13 for a point source (where $y_{w0} = 0$ at $x_0 = 0$). Figure 6b compares the scaling for the moving surface by showing the change in the width of the wetted region with distance down the slope for a fixed belt speed, over a range of volume fluxes of fluid. The data in Figure 6b collapse onto the curve expected from Eq. 30 and there appears to be no systematic deviation from the expected behavior with belt speed, which indicates that the correct physical processes are captured by the model. Figure 6c shows the variation of the width of the flow with belt speed and volume flow rate at a fixed distance down the slope. Here an offset to take into account the finite size of the liquid source in the experiments could not be applied because it requires information about the width for different distances from the source. Despite this, good agreement with the similarity solution for high belt speed is found, as shown in Figure 6c. As the belt speed decreases, the predictions and measurements diverge from each other. This is expected because the fluid then begins to flow down the inclined surface rather than being wholly advected with it.

Motion of the Liquid Close to the Pinch Bar. The measured dimensions of the liquid flow are shown in Figure 7a as a function of surface speed for fixed volume flux and compared with the low *Re* description of the flow. The variation of the three dimensions of the fluid layer adjacent to the pinch bar —$h_m(0)$, $x_m(0)$, y_m—with increasing belt speed is shown in Figure 7a as a function of surface speed with the volume flux fixed at $Q = 7.7 \times 10^{-5}$ m^3/s. The shrinkage of all three dimensions of the pool with increasing belt speed is predicted well, even though the assumption that the pool is a free-surface gravity flow is less well founded at higher belt speeds. Figure 7b shows how the dimensions of the wetted region change with increasing volume flux of liquid for a fixed belt speed of $U = 0.16$ m/s, and the increase in dimensions with Q is confirmed by predictions (Eqs. 17, 23 and 24).

The variation in total travel time of the fluid from the source until it has passed under the pinch bar with belt speed was studied for two volume flow rates. The results are plotted in Figure 8 with the theoretical predictions, and fair agreement is observed. As the belt speed increases, the travel time decreases and becomes less dependent on the volume flow rate. Above $U > 0.35$ m/s, the difference between the travel time for both flow rates decreases because T_2 decreases more rapidly with U than the advective time T_1 (which is independent of Q), and this is confirmed experimentally. The travel time from the source to the pinch bar, $T_1 = d/U$, is plotted in Figure 8, where $d = 0.65$ m. Comparison with experimental measurements shows that the advective component of the total travel time decreased from 60% at low belt speed to 50% at higher belt speeds.

Structure of the Flow. The flow structure close to the pinch bar could be seen in recordings of the flow there. The flow imaging technique clearly showed the streak lines, particularly because the flow is laminar owing to the high fluid viscosity. Figure 9 is an oblique view of the fluid flow down the moving surface and spread parallel to the pinch bar. Figure 10 shows the complex structures that can form close to the pinch bar and depend on belt speed. At all belt speeds the fluid traveled along the lower belt until its forward motion was resisted and retarded by the restriction at the pinch bar. The fluid is forced back with increasing vigor as the belt speed increases, forming the complex stepped structures seen in the figure. The fluid close to the lower belt passes straight underneath the pinch bar; however, the rest of the fluid forms a longitudinal, horizontal vortex whose axis is parallel to the pinch bar. The fluid is forced sideways by the hydrostatic pressure gradient, and the streak lines circulate in a sawtooth pattern, as sketched in Figure 11a. The shape is caused by the moving belt, which continues to advect fluid under the pinch bar, so that when fluid nears the bottom of the flow it moves in a straight line toward the pinch bar as shown in Figure 11b. This vortex appears to have a regular pattern up to the edges of the pool. Figure 11c shows the pattern generated when tracer particles are added to the viscous fluid. Some of the tracer particles become trapped in convergence zones in the surface flow of the viscous pool, which appear as a dark curve.

Optimal Operating Conditions for the Industrial Process

The mathematical description provides a leading order description of the flow conditions and may be applied to optimize the industial process. Two constraints can be applied to the industrial process. The first is that wastage of the materials used in the manufacture process is minimized and this

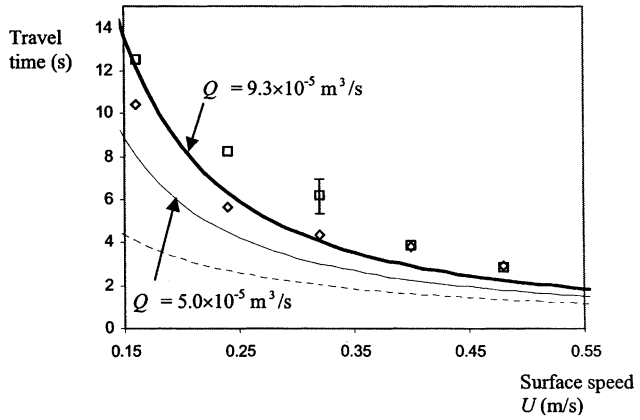

Figure 8. Predicted total travel time T of the fluid (solid lines) from Eq. 29 vs. experimental measurements for two values of the volume flux, Q: 9.3×10^{-5} m/s (□); 5.0×10^{-5} m^3/s (◇).

The dashed curve corresponds to the advective component of the residence time, T_1. The typical experimental error is shown.

constraint requires that the width of the wetted region y_m is fixed and corresponds to the width of the final laminated sheet. The second condition is that the maximum travel time is less than the time taken for the filler to solidify, T_s.

The width of the wetted region, $y_m = Q/2Ua$, is fixed and this provides a relationship between the volume flux of fluid added and the belt speed. The condition that the travel time is less than T_s, according to Eq. 29, reduces to

$$T_s - \frac{d}{U} - \frac{147}{32}\frac{2^{8/6}y_m^{8/7}}{a^{3/7}U^{6/7}}\left(\frac{\mu}{\rho g}\right)^{1/7} \geq 0 \qquad (31)$$

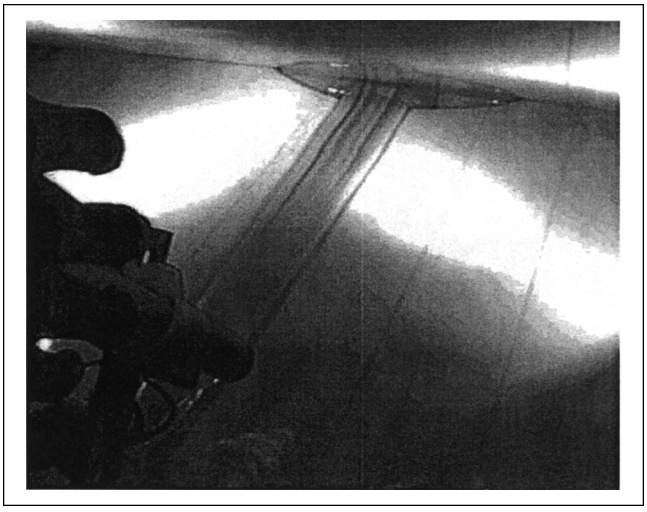

Figure 9. Oblique view of the dye streak lines introduced into the viscous fluid.

The volume flux is $Q = 9.3\times10^{-5}$ m^3/s and the belt speed is $U = 0.16$ m/s. The dye lines are used to measure the fluid travel times, but also give qualitative insight into the flow features.

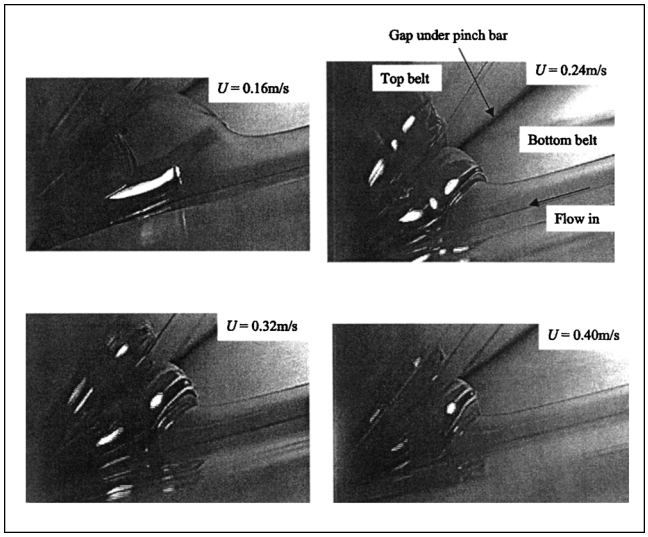

Figure 10. Experimental observations of the flow features close to the pinch bar where the volume flux of fluid is fixed ($Q = 9.3\times10^{-5}$ m^3/s) and the belt speed is progressively increased.

where the volume flux has been eliminated with $Q = 2Uay_m$. When the width of the laminated sheet is narrow (or the belt speed high), the total travel time is dominated by advection to the pinch bar, so that

$$U = \frac{d}{T_s} \qquad (32)$$

This constraint is independent of the width of the manufactured laminated sheet. When the manufactured sheet is wide (or the belt speed slow), the total travel time is dominated by advection parallel to the pinch bar and

$$U = \left(\frac{147}{32}\right)^{7/6}\frac{2^{4/3}}{a^{1/2}}y_m^{4/3}\left(\frac{\mu}{\rho g}\right)^{1/6} \qquad (33)$$

Numerical solutions to Eq. 31 can be developed for intermediate values of y_m. Figure 12a shows how the optimal speed of the sheet varies with the half-width of the final product, for various values of solidification times ($T_s = 10$, 15, 20 s). The fluid viscosity and density taken corresponded to experimental conditions and the pinch-bar separation was $a = 1.5\times10^{-3}$ m. An important result is that under typical manufacturing conditions the time associated with advection from the source to the pinch bar is small compared to the contribution due to transport along the pinch bar, because the width of the wetted region is typically much larger than obtained under laboratory operating conditions. Figure 12b shows how the optimal belt speed varies with the pinch-bar separation (a) from 1×10^{-3} to 2.5×10^{-3} m. The pinch-bar separation has a significant effect on travel time and on the optimal belt speed.

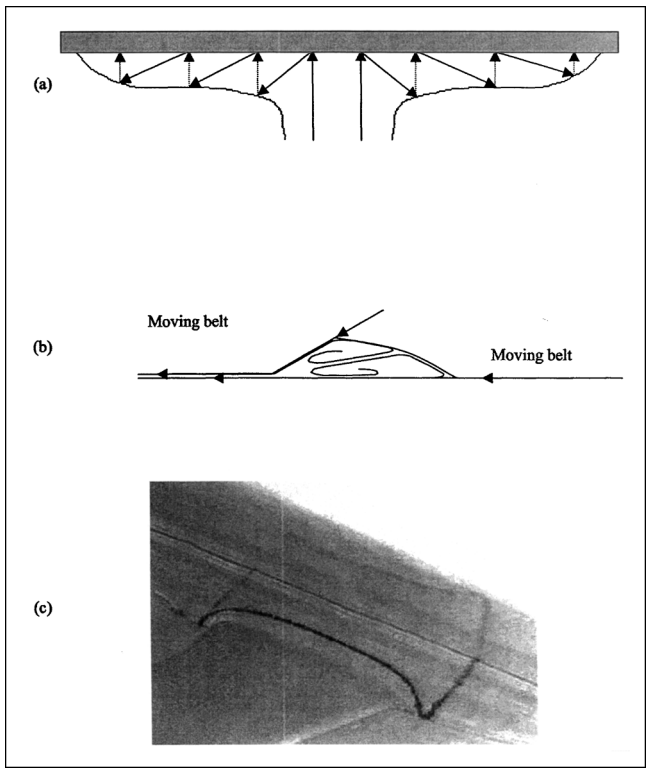

Figure 11. (a) Streaklines generated by the dye source; (b) 3-D streamline pattern; (c) experimental observations of opaque tracer particles introduced into the flow (particles appear to accumulate along stagnation lines on the surface of the pool).

The dye followed a path whereby it traveled outwards and away from the pinch bar in the upper parts of the pool of liquid until it reached the back of the pool of liquid where it approached the moving belt, which quickly pulled it back to the pinch bar. This path can be seen in Figure 9.

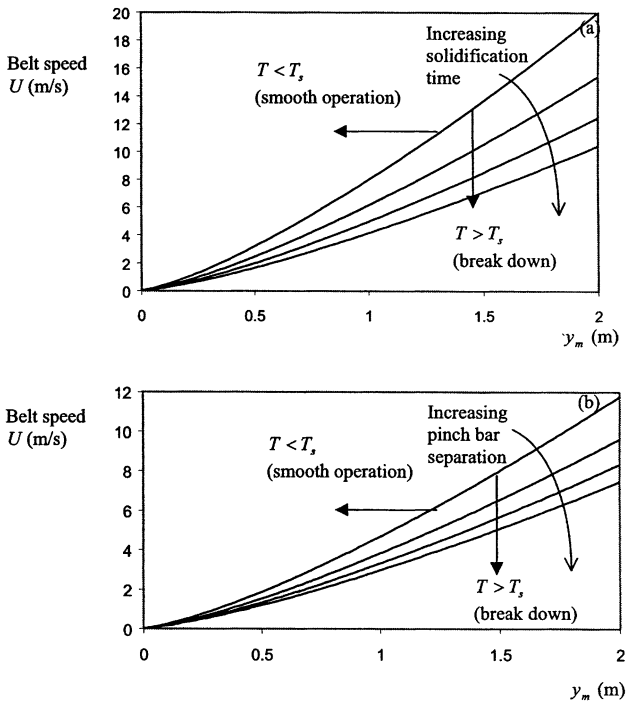

Figure 12. Optimal operating speed for the moving belts.

The optimal solution is determined from the condition that the width of the manufactured board (y_m) is fixed and the setting time is known, and is plotted in (a). The setting times are $T_s = 8$, 10, 12 and 14. The effect of the separation of the moving belts under the pinch bar on the optimal belt speed is shown in (b), where the setting time is fixed at $T_s = 15$ s and the pinch bar separation is $a = 1$, 1.5, 2.0 and 2.5 mm. The fluid properties correspond to those used in the experimental study and represent values typical of the industrial process.

Concluding Remarks

This article describes a detailed experimental and theoretical study of the spreading of viscous fluid down a moving rigid surface and parallel to a pinch bar, both processes that are important in manufacturing laminated sheets. A new description of viscously dominated flow in both of these situations has been developed and in both cases very good agreement was observed between experimental measurements of the rate of spreading of the fluid and theoretical predictions. The theoretical predictions do not contain adjustable parameters, and the agreement suggests that the models capture the key physical processes. The main results are summarized in Tables 2 and 3. Experimental measurements of the travel time of the fluid are in fair agreement with theoretical predictions. The travel time of the fluid from its source until it has passed under the pinch bar is a combination of the ad-

Table 2. Scalings for Viscous Flow Down a Moving Surface

Flow down a fixed surface	$Y \sim \left(\frac{3\mu Q \cot^3\theta}{4\rho g \sin^4\theta}\right)^{1/7} x^{3/7}$ $\quad H \sim \left(\frac{3\mu Q}{\rho g \cos\theta}\right)^{2/7} x^{-1/7}$	$x_1 \ll x \ll x_*$ (Lister, 1992)
Flow down a moving surface	$Y \sim \left(\frac{5\rho g Q^3 \cos\theta}{24\mu U^4}\right)^{1/5} x^{1/5}$ $\quad H \sim \left(\frac{3\mu Q^2}{20 U \rho g \cos\theta}\right)^{1/5} x^{-1/5}$	$x \gg x_*$ (This study)

Table 3. Scalings for Flow Parallel to Pinch Bar

$Re \ll 1$	$y_m = \dfrac{Q}{2Ua}$
	$x_m \sim \dfrac{1}{9}\left(\dfrac{63}{2}\right)^{3/7}\left(\dfrac{\rho g}{\mu}\right)^{1/7}\dfrac{Q^{6/7}}{a^{3/7}U}$
	$h_m \sim \left(\dfrac{63}{2}\right)^{1/7}\left(\dfrac{\mu}{\rho g}\right)^{2/7}\dfrac{Q^{2/7}}{a^{1/7}}$

vection time, T_1, from the source to the pinch bar and the time, T_2, taken for it to flow parallel to the pinch bar. The total travel time in the experiments was larger than that anticipated from the vertically averaged formulation. This may be because of a number of different factors. The complex interaction between the downslope flow and the flow parallel to the pinch bar was neglected in this treatment, but this will become less important as the width of the downslope flow near to the pinch bar decreases when compared to y_m. In addition, there are a number of complex flow structures in the real flow that may increase the travel time.

The mathematical description has been used to determine the optimal operating speed of the industrial process. This is a function of the width of the final product, pinch-bar separation, and the properties of the viscous fluid. These results indicate that under typical industrial conditions the total travel time is dominated by transport parallel to the pinch bar.

There are a number of extensions to the present study that can be considered. A reduction in the travel time would require changing the pinch-bar geometry or the introduction of additional sources of fluid. Multiple sources will reduce the travel time because the effective width of the board to be covered by a single source (y_m) is reduced and this effect can be calculated from this description. The effect of pinch-bar geometry, such as the tilt of the lower surface to promote pooling of fluid, is complex and would require the introduction of additional physical effects neglected in the current treatment. The effect of the changed fluid properties with time plays an important role in an industrial context. The viscosity of the setting fluids increases rapidly with time and this would tend to increase both the height (h_m) and decrease the width of the pool (x_m) before the pinch bar, although the travel time is weakly dependent on the fluid viscosity, which is raised to the power of 1/7.

Acknowledgments

The authors gratefully acknowledge the technical contribution and support of S. O'Nien of EUTECH, ICI, and the work of N. Hale, T. Rhys, D. Wigley, and A. Seal, all formerly of the Department of Mechanical Engineering of the University of Bristol, in designing and building the experimental apparatus, and the support of the Graduate School at UCL for the purchase of video equipment. One of the authors (I.E.) gratefully acknowledges the support of a Research Fellowship by the Leverhulme Trust at Bristol University and by the E.P.S.R.C. at University College London.

Literature Cited

Bercovici, D., "A Theoretical Model of Cooling Viscous Gravity Currents, With Temperature Dependent Viscosity," *Geophys. Res. Lett.*, **21**, 1177 (1994).

Didden, N., and T. Maxworthy, "The Viscous Spreading of Planar and Axisymmetric Gravity Currents," *J. Fluid Mech.*, **121**, 27 (1982).

Huppert, H., "The Propagation of Two-Dimensional and Axisymmetric Viscous Gravity Currents Over Rigid Horizontal Surface," *J. Fluid Mech.*, **121**, 43 (1982a).

Huppert, H., "Flow and Instability of a Viscous Current Down a Slope," *Nature*, **300**, 427 (1982b).

Lister, J., "Viscous Flows Down an Inclined Plane from Point and Line Sources," *J. Fluid Mech.*, **242**, 631 (1992).

Myers, T., "Thin Films with Surface Tension," *Soc. Ind. Appl. Math. Rev.*, **40**, 441 (1998).

Manuscript received Aug. 20, 2001, and revision received Mar. 15, 2002.